Notes on modeling for Kerr black holes: Basis learning, QNM frequencies, and spherical-spheroidal mixing coefficients

L. London[1]

[1]*School of Physics and Astronomy, Cardiff University, The Parade, Cardiff, CF24 3AA, United Kingdom*

(Dated: June 18, 2018)

The ongoing direct detection of gravitational wave signals is aided by representative models of theoretical predictions. In particular, the process of model based detection, and subsequent comparison of signals the general relativity's predictions are aided by the modeling of information related to perturbed Kerr black holes. Here, we summarize recent methods and models for the analytically understood gravitational wave spectra (quasi-normal mode frequencies), and harmonic structure of Kerr black holes (mixing coefficients between spherical and spheroidal harmonics). Towards the construction of these models, two algorithms, GMVP and GMVR, for the automated polynomial and rational modeling of general dimensional complex scalars are presented.

I. INTRODUCTION

In the coming years, expectations for frequent Gravitational wave (GW) detections of increasing signal-to-noise ratio (SNR) are high. Concurrent with Virgo, the Advanced LIGO (aLIGO) detectors will enter their third observing run in late 2018. At this time, binary black hole (BH) detections are expected at a rate of X per month. In this context, signal detection and subsequent inference of physical parameters hinges upon efficient models for source properties and dynamics. Most prominently, there is ongoing interest in signal models for binary BH inspiral, merger and ringdown (IMR). As the merger of isolated BHs is expected to result in a perturbed Kerr BH, there is related interest in having computationally efficient models for perturbative parameters, namely those that enable evaluation of the related ringdown radiation.

In particular, a perturbed Kerr BH (e.g. resulting from binary BH merger) will have GW radiation that rings down with characteristic frequencies, $\tilde{\omega}_{\ell mn} = \omega_{\ell mn} + i/\tau_{\ell mn}$. These discrete frequencies have associated radial and spatial functions which are *spheroidal* harmonic in nature. These frequencies and harmonic functions are the so-called Quasi-Normal Modes (QNMs). They are the eigen-solutions of the source free linearized Einstein's equations (i.e. Teukolsky's equations) for a perturbed BH with final mass, M_f, and dimensionless final spin, j_f. The well known and effective completeness of these solutions allows gravitational radiation from generic perturbations to be well approximated by a spectral (multipolar) sum which combines the complex QNM amplitude, $A_{\ell mn}$, with the spin weight -2 spheroidal harmonics, ${}_{-2}S_{\ell mn}$.

$$\begin{aligned} h &= h_+ - i\, h_\times \\ &= \frac{1}{r}\sum_{\ell mn} A_{\ell mn}\, e^{i\,\tilde{\omega}_{\ell mn} t}\, {}_{-2}S_{\ell mn}(j_f \tilde{\omega}_{\ell mn}, \theta, \phi) \\ &= \frac{1}{r}\sum_{\bar{\ell}\bar{m}} h_{\bar{\ell}\bar{m}}(t)\, {}_{-2}Y_{\bar{\ell}\bar{m}}(\theta, \phi)\ . \end{aligned} \tag{1}$$

In the first and second lines of Eqn. (1), we relate the observable GW polarizations, h_+ and $h_\times$, with the analytically understood morphology of the time domain waveform. Here, the labels ℓ and m are eigenvalues of Teukolsky's angular equations, where units of $M = 1$ (e.g. the initial mass of the binary BH system), and $c = 1$. In the third line of Eqn. (1), we represent h in terms of *spherical* harmonic multipoles. This latter form is ubiquitous for the development and implementation of IMR signal models for binary BHs.

Towards the development of these models, Eqn. (1) enters in many incarnations. In the Effective One Body (EOB) formalism, $h_{\bar{\ell}\bar{m}}$ is modeled such that, after its peak (near merger), the effective functional form reduces (asymptotically) to Eqn. (1)'s second line. This view currently comes with the added assumption that ${}_{-2}S_{\ell mn} = {}_{-2}Y_{\ell m}$, where only $n = 0$ is explicitly considered. The consequences of this choice are discussed in reference [X]. For the so-called *Phenom* models, the frequency domain multipoles, $\tilde{h}_{\bar{\ell}\bar{m}}(f)$, are constructed such that their high frequency behavior is consistent with Eqn. (1) in the time domain.

Both Phenom and EOB approaches directly use phenomenological models (i.e. fits) for the QNM frequencies, as these fits are more computationally efficient than the underlying analytic calculations, which involve the solving of continued fraction equations. In the case of `PhenomHM` and derivative models, fits for the QNM frequencies are used in the process of mapping $\tilde{h}_{22}(f)$ into other $\tilde{h}_{\bar{\ell}\bar{m}}(f)$ [X]. In that setting, the QNM frequencies impact the morphology of each $h_{\bar{\ell}\bar{m}}$ in not only ringdown, but also merger and late inspiral.

For models that assist tests of the No-Hair Theorem, and thereby only include precise ringdowns, the perspective of Eqn. (1)'s second and third lines are used to write each spherical harmonic multipole moment as

$$h_{\bar{\ell}\bar{m}} = \frac{1}{r}\sum_{\ell mn} A_{\ell mn} e^{i\tilde{\omega}_{\ell mn} t} \sigma_{\bar{\ell}\bar{m}\ell mn} \tag{2}$$

where, the spherical-spheroidal mixing coefficient, $\sigma_{\bar{\ell}\bar{m}\ell mn}$, is

$$\sigma_{\bar{\ell}\bar{m}\ell mn} = \int_\Omega {}_{-2}S_{\ell mn}\, {}_{-2}Y^*_{\bar{\ell}\bar{m}}\, \mathrm{d}\Omega\ . \tag{3}$$

In Eqn. (3), $*$ denotes complex conjugation, and Ω is the standard solid angle in spherical polar coordinates.

In practice, Eqn. (2) is computationally efficient: The calculation of each ${}_{-2}S_{\ell mn}$ involves a series solution which slowly converges for j_f near unity. Therefore, it is more effective to have accurate models for $\sigma_{\bar{\ell}\bar{m}\ell mn}$, which can then be used directly to calculate $h_{\bar{\ell}\bar{m}}$ via Eqn. (2), and thereby the GW polarizations via Eqn. (1).

In this combined context, it is clear that the modeling of QNM frequencies, $\tilde{\omega}_{\ell mn}$, and spherical-spheroidal mixing coefficients, $\sigma_{\bar{\ell}\bar{m}\ell mn}$, underpin a wide range of GW signal models. While models for $\tilde{\omega}_{\ell mn}$ and $\sigma_{\bar{\ell}\bar{m}\ell mn}$ are present in many publications, there exist minor shortcomings which we wish to address here.

For the QNM frequencies, it is well known that for nearly

extremal BHs (i.e. $j_f \to 1$) some of the frequencies have zero-damping (i.e. $\tau_{\ell mn} \to \infty$). In the context of aLIGO data analysis, where source parameters are estimated using routines which sample over the space of possible BH masses and spins, it is useful to have accurate physical behavior in the extremal limit. Here, we present the first models for $\tilde{\omega}_{\ell mn}$ that explicitly account for zero-damping in the extremal Kerr limit.

For the modeling of $\sigma_{\bar{\ell}\bar{m}\ell mn}$, we note that the results presented in [X] are limited to cases where the azimuthal indices, ℓ and $\bar{\ell}$, are less than or equal to 3. As the most advanced signal models include at least ℓ or $\bar{\ell}$ of 3, there is use in extending prior results. In particular, it is well known that σ_{43330} can have a significant impact on the (4, 3) spherical multipole. For consistency with the multipolar content of current ringdown models, here, we extend previous results to include the most significant multipoles with $\ell \leq 5$.

In parallel, the methods for modeling $\tilde{\omega}_{\ell mn}$ and $\sigma_{\bar{\ell}\bar{m}\ell mn}$ have been dispersed: different phenomenological techniques have been used under no coherent framework. Here we will present linear modeling techniques, namely the greedy-multivariate-polynomial (`GMVP`) and greedy-multivariate-rational (`GMVR`) algorithms, in which model terms are iteratively learned with no initial guess. The description of `GMVP` given here is complementary to similar algorithms used to model QNM excitation amplitudes, $A_{\ell mn}$, as present in reference [cite]. As we will discuss, the `GMVR` algorithm is an iterative approach to the (pseudo) non-linear modeling of multivariate rational functions. Both `GMVP` and `GMVR` are intended for use with low noise data (e.g. the results of analytic calculations), and each employs a reverse (or negative) greedy algorithm to counter over modeling. As the underlying process for `GMVP` and `GMVR` is stepwise regression, highly correlated basis vectors (i.e. polynomial terms) are handled via an approach we will call *degree tempering*. It will be demonstrated that these approaches are readily capable of modeling the complex valued $\tilde{\omega}_{\ell mn}$ and $\sigma_{\bar{\ell}\bar{m}\ell mn}$. Results suggest that the versions of `GMVP` and `GMVR` presented here may have broad application in instances where training data are approximately noiseless, and an initial guess is difficult to obtain.

The plan of the paper is as follows. In section Section (II), we outline the `GMVP` and `GMVR` algorithms. In Section (III), we demonstrate the application of each algorithm. We first consider the application of `GMVP` to the modeling of QNM frequencies. We then consider the application of `GMVR` to the modeling of spherical-spheroidal mixing coefficients. In Section (IV), we review the performance of `GMVP` and `GMVR`, and we discuss potential applications for these methods.

II. METHODS

Within the topic of regression, linear regression has particular advantages: its matrix based formulation can be computationally efficient, and it does not require initial guesses for model parameters. Perhaps most intriguingly, the formal series expansions of smooth functions support linear and rational models (e.g. Pade approximants) having application to many datasets. Here we will develop algorithms for the linear modeling of scalar functions (real or complex valued) of many variables.

If we consider a scalar function, f, of N variables sampled in j, $\vec{x}_j = \{x_{\alpha j}\}_{\alpha=0}^{N}$, then $f(\vec{x})_j$ can be represented (possibly inaccurately) as a sum over K linearly independent basis functions, $\phi_k(\vec{x}_j)$:

$$f(\vec{x})_j \;=\; \sum_{k=0}^{K} \mu_k \, \phi_{kj} \; . \tag{4}$$

The central player is Eqn. (4) is the set of basis coefficients μ_k. Typically, one chooses or derives $\phi_k(\vec{x}_j)$ to capture inherent features of $f(\vec{x}_j)$. With $\phi_k(\vec{x}_j)$ assumed to be known, the linear representation (Eqn. 4) lastly defined by the set of μ_k.

From here it is useful to note that Eqn. (4) has a linear homogeneous matrix form. In particular, defining $\hat{U} = \{\phi_{kj}\}$, and $\vec{f} = \{f_j\}$, then $\vec{f} = \hat{U}\,\vec{\mu}$. This implies that

$$\vec{\mu} = \hat{P}\,\vec{f}\,, \tag{5}$$

where

$$\hat{P} = \left(\left(\hat{U}^{-1}\right)^T \hat{U}^{-1}\right)^{-1} \tag{6}$$

is the *pseudo-inverse* of $\hat{U}$. Equations (4), and related discussion through Eqn. (6) illustrate the most rudimentary solution to the linear modeling problem. However, there are many ways to expand upon and refine the solution presented thus far. In the following subsections we will consider two such approaches. First we will consider the general polynomial modeling of multivariate scalar functions. This will encompass the `GMVP` algorithm. Second, we will build upon the `GMVP` approach by considering models of rational functions: polynomials divided by polynomilas. To consider these two approaches in a largely automated way (i.e. where the set of possible basis functions is known, but the select basis functions ultimately used are *learned*), we will make use of the *greedy* algorithm approach.

A. A Generic Greedy Algorithm

While we most often want a single model for a given dataset (e.g. some approximation of $\vec{f}$ from numerical calculation or experiment), there are often many more modeling choices than desired. In particular, if we refer to our set of all possible basis functions as our "*symbol space*", then the problem of determining how many, and which basis vectors (i.e. symbols) to use is a problem of combinatoric complexity.

A well known method for finding an approximate solution to this problem is the so-called "greedy" algorithm. The premise is this: We will iteratively construct models with increasing number of symbols. The process begins by finding the single symbol (basis vector) that yields the most accurate model (in the sense of minimizing least-squares error). That encompasses the first iteration of a process in which we will greedily add symbols to our model. In each following iteration, an all remaining symbols are added to the model one at a time, and the single additional symbol which yields the greatest increase in model accuracy is kept for the following iteration. In this way, a list of optimal model symbols is learned. The forward process is to end when the model accuracy (or changes thereof) pass a specified threshold. This rough algorithmic picture encapsulated in Alg. 1.

Note that we will use the terms "basis vector" and "model symbol" interchangeably. However, in practice, it can be use-

ful to represent basis vectors symbolically (e.g. with strings), and have a way of bijectively mapping between symbols and numerical basis vectors.

Algorithm 1 A positive (forward) greedy algorithm, `PGREEDY`, `PGREEDY`. Note that a required input, $\mathcal{A}$, is a function that takes in a list of basis symbols, and outputs an estimator of fit error. In this setting, $\mathcal{A}$ is assumed to have access to peripheral information, such as the training data.

Input: $\{\boldsymbol{\lambda}_{bulk}$ = basis symbols, $\mathcal{A}$ = action, tol = greedy tolerance$\}$
Define empty list of kept symbols: $\boldsymbol{\lambda}_{kept} = \{\}$
Initialize estimator value and loop boolean: ϵ_{last} = inf, $done$ = False
while not $done$ **do**
  $\epsilon_{min} = \epsilon_{last}$
  for $\boldsymbol{\lambda}$ in $\boldsymbol{\lambda}^{bulk}$ **do**
    $\boldsymbol{\lambda}_{trial} = \boldsymbol{\lambda}_{kept} \cup \boldsymbol{\lambda}$ (add $\boldsymbol{\lambda}$ to $\boldsymbol{\lambda}_{kept}$)
    $\epsilon = \mathcal{A}(\boldsymbol{\lambda}_{trial})$ (action returns fit error)
    if $\epsilon < \epsilon_{min}$ **then**
      $\epsilon_{min} = \epsilon$ (store trial min)
      $\boldsymbol{\lambda}_{min} = \boldsymbol{\lambda}_{trial}$
    end if
  end for
  $done = |\epsilon_{min} - \epsilon_{last}| < tol$
  if not $done$ **then**
    $\epsilon_{last} = \epsilon_{min}$
    $\boldsymbol{\lambda}_{kept} = \boldsymbol{\lambda}_{kept} \cup \boldsymbol{\lambda}_{min}$ (update kept symbols)
  end if
end while
Output: $\{\boldsymbol{\lambda}_{kept}\}$ (the Greedy Basis)

B. Greedy Multivariate Polynomial Fitting

The study of smooth scalar functions (e.g. $\vec{f}$) often centers about the Taylor series expansion. In that instance, it is clear that any infinitely differentiable scalar function of many variables can be represented in terms of its derivatives by

$$f(\vec{x}+\vec{h}) = e^{\vec{x}\cdot\vec{\nabla}'} f(\vec{x}')|_{\vec{x}'=\vec{h}} \approx \sum_{k=0}^{K} \frac{1}{k!} (\vec{x}\cdot\vec{\nabla}')^k f(\vec{x}')|_{\vec{x}'=\vec{h}} \quad (7)$$

From the first to second line of Eqn. (7), we have used the definition of the exponential function (i.e. its series expansion form). In the second line, the equality has been replaced by an approximation as we have limited the linear representation to K terms. This latter point is key to the perspective of `GMVP`: given training data thought to be related to a smooth multivariate function, it may be well approximated by a truncated series expansion in the appropriate coordinate basis.

This truncated expansion happens to be a polynomial in at most N variables. In this setting, the uncertainty of which and how many basis terms to include makes this a problem ripe for the application of Eqn. (5) and Alg. (1) .

In the current setting, the basis symbols required by Alg. (1) are the multinomial terms in Eqn. (7). Each term is an element of the n-fold cartesian inner-product of the power-sets of each model dimension. That is $\boldsymbol{\lambda}_{bulk} = \{x_0, x_1 ... x_N, ... x_0^1, x_0^2, x_0^3, ..., (x_0^K x_1^K ... x_N^K)\}$. Note that in practice it may be useful to encode elements of $\boldsymbol{\lambda}_{bulk}$ with strings representing their constituents (e.g. $x_0 x_0 x_1 x_2 x_2 x_4$ could be represented by the string "001224").

The action, $\mathcal{A}(\boldsymbol{\lambda}_{trial})$, required by Alg. (1) encompasses the evaluation of Eqn. (5) to solve for the basis coefficients, μ_k, and the calculation of the modeling error. An explicit sktech of this is given by Alg. (2).

Algorithm 2 $\mathcal{A}_{\texttt{GMVP}}$, the action for `GMVP`. Model calculation given basis symbols, and output of model error estimate.

Input: $\boldsymbol{\lambda}_{trial}$
Calculate μ_k via Eqn. (5).
Calculate the model representation error, e.g.: $\epsilon = |var(\hat{U}\vec{\mu} - \vec{f})|/var(\vec{f})$, where var is the variance of the respective list.
Output: ϵ

The combination of these two ideas alone results in an algorithm prone to a deficit of stepwise methods: the algorithm may confuse correlated basis vectors (e.g. x^2 may be confused for x^4). To counter this, we may incrementally increase, or *temper*, the maximum allowed multinomial order. Recall that a term such as $x_0 x_1 x_3^2$ has an effective degree of 4. The combination of degree tempering with the greedy approach results in the `GMVP` algorithm as presented in Alg. (3).

Algorithm 3 `GMVP`, a degree tempered stepwise algorithm for multivariate polynomial modeling of scalar data.

Input: $\{x, f$,max_degree $= 6, tol\}$
Define, $\boldsymbol{\lambda}_{bulk}$, the bulk symbol space using the n-fold cartesian inner-product of the power set of each basis symbol
Define $\mathcal{A}_{\texttt{GMVP}}$ according to Alg. (2).
Given max_order, define, D, a list of allowed polynomial degrees (e.g. $\{0, 1, 2, 3, 4, 5, 6\}$)
for d **in** D **do**
  Define $\boldsymbol{\lambda}_{bulk}^{(d)}$ as all symbols from $\boldsymbol{\lambda}_{bulk}$ with degree less than or equal to current degree: $\boldsymbol{\lambda}_{bulk}^{(d)}$
  Using $\boldsymbol{\lambda}_{bulk}^{(d)}$, apply Alg. (1), `PGREEDY`, with $\mathcal{A}_{\texttt{GMVP}}$ to get symbol subset, $\boldsymbol{\lambda}_{opt}^{(d)}$ and estimator val, $\epsilon_{opt}^{(d)}$
  if $|\boldsymbol{\lambda}_{opt}^{(d)} - \boldsymbol{\lambda}_{opt}^{(d-1)}| < tol$ **then**
    break
  end if
end for
Output: $\boldsymbol{\lambda}_{opt}^{(d)}$

C. Greedy Multivariate Rational Fitting

Despite the apparent universality of of Eqn. (7), there are many cases where K must be orders of magnitude greater than 1 in order for $\vec{f}$ to be accurately represented by a multinomial (historically, this is equivalent to "Runge's phenomenon"). Of

the simplest examples are the rational functions of the form

$$f(\vec{x}) = \bar{\mu} + \bar{\sigma}_f \, \frac{\sum_{r=0}^{R} a_r \, \phi_r(\vec{x})}{1 - \sum_{v=1}^{V} b_v \, \phi_v(\vec{x})} \, , \tag{8}$$

where $\bar{\mu}$ is the additive mean of $f(\vec{x})$, and $\bar{\sigma}_f$ is the standard deviation of $f(\vec{x})$ from its mean, and ϕ_k are the multinomials basis functions considered in the previous section. Note that, in Eqn. (8), the sum over v does not include the constant term associated with ϕ_0.

While it is tempting to embrace Eqn. (8)'s $f(\vec{x})$ as a nonlinear function and so resort to nonlinear modeling methods, a reformulation reveals an underlying linear structure. Namely, if we let

$$g = (f - \bar{\mu})/\bar{\sigma}_f \tag{9}$$

then the algebraic manipulation of Eqn. (8) results in

$$g = \sum_{r=0}^{R} a_r \, \phi_r(\vec{x}) + g \sum_{v=1}^{V} b_v \, \phi_v(\vec{x}) \, . \tag{10}$$

We are free to relabel the indices such that Eqn. (10) is manifestly linear in a single index. At this stage, we will also explicitely consider the j^{th} samples of the domain, and so refer to $\vec{x}$ as $\vec{x}_j$. The adjustments of perspective result in

$$g_j = \sum_{k=0}^{R+V+1} z_k \, \psi_k(\vec{x}_j) \, , \tag{11}$$

where

$$z_k = \left\{ \begin{array}{ll} a_k, & \text{for } 0 \leq k \leq R \\ b_k, & \text{for } R+1 \leq k \leq R+V \end{array} \right\} \tag{12}$$

and

$$\psi_k(\vec{x}_j) = \left\{ \begin{array}{ll} \phi_k(\vec{x}_j), & \text{for } 0 \leq k \leq R \\ \phi_k(\vec{x}_j) \, g, & \text{for } R+1 \leq k \leq R+V \end{array} \right\} \tag{13}$$

Recalling Equations (5)–(6), it follows that the coefficients of interest (a_k and b_k), may be estimated according to

$$\vec{\alpha} = \hat{P} \, \vec{g} \, . \tag{14}$$

where, here, $\hat{P}$ is the pseudo-inverse of the matrix whose elements are $\psi_k(\vec{x}_j)$.

However, we note that $\hat{P}$'s depending on g signals that there is more to be done. In particular, let us briefly consider the effect of zero-mean noise on g, e.g. $g \to g + n$. In this contemplation, it may be that shown that n may be entirely regelated to $\hat{P}$. It is in this sense that Eqn. (14) is insufficient to generally solve for $\vec{\alpha}$.

The key to robustly solving for $\vec{\alpha}$ lies in the iterative refinement of $\vec{\alpha}$. Specifically, we note that Eqn. (10) may be modified to iteratively minimize the impact of numerical noise on $\hat{P}$. That is, to reduce the impact of noise on $\hat{P}$, we are free to calculate it using model evaluations of g rather than the original training data. To this end, if we define $g^{(0)} = g$ (i.e. the training data) then, with $\hat{P} = \hat{P}(\vec{g}^{\,(n)})$, Eqn. (14) generalizes to

$$\vec{\alpha}^{(n+1)} = \hat{P}(\vec{g}^{\,(n)}) \, \vec{g}^{(0)} \, . \tag{15}$$

In practice, one solves Eqn. (15) for $\vec{\alpha}^{(n)}$, and then uses the related $a_r^{(n)}$ and $b_v^{(n)}$ to calculate $g^{(n+1)}$ via

$$g^{(n+1)} = \frac{\sum_{r=0}^{R} a_r^{(n+1)} \, \phi_r(\vec{x})}{1 \; - \; \sum_{v=1}^{V} b_v^{(n+1)} \, \phi_v(\vec{x})} \, , \tag{16}$$

which is then fed back into Eqn. (15) for further refinement. The refinement process is to terminate when a measure of model error (e.g. $||g^{(0)} - g^{(n)}||$) passes a predetermined threshold.

Much as in the case of multivariate polynomial fitting, we are left with an un unknown number and content of basis symbols. In principle, the existence of a_r and b_v makes the problem more complicated, as one could imagine optimizing over each symbol space independently. To broach these complications, we again use a greedy algorithm with degree tempering. However, rather than independent greedy optimizations for the numerator and denominator bases symbols, Eqn. (11) suggests that the appropriate labeling of symbols (e.g. "numerator" or "denominator") may yield an effective flattening of the supposed 2D basis selection problem. Put another way, rather than two greedy optimizations over R and $V-1$ symbols (with $(V-1)R$ iterations), a single greedy process over $V+R$ symbols is performed.

With the conceptual tools in hand, we may proceed to constructing `GMVR` by first defining its action, $\mathcal{A}_{\texttt{GMVR}}$. This is done in Alg. (4).

Algorithm 4 $\mathcal{A}_{\texttt{GMVR}}$, the action for `GMVR`. Model calculation given basis symbols, and output of model error estimate.

Input: $\{ \boldsymbol{\lambda}_{trial}, tol = 10^{-3} \}$
Calculate $\alpha_k^{(1)}$ via Eqn. (15). Implicitly, $n = 1$.
Calculate the current model prediction $g^{(1)}$ via Eqn. (16).
Calculate the model representation error, e.g.: $\epsilon^{(1)} = |var(g^{(n)} - g^{(0)})|/var(g^{(0)})$.
$done = False$
while not $done$ **do**
    Calculate α_k^{n+1} via Eqn. (15).
    Calculate the current model prediction $g^{(n)}$ via Eqn. (16).
    Calculate the model representation error, e.g. $\epsilon^{(n)} = |var(g^{(n)} - g^{(0)})|/var(g^{(0)})$.
    $done = |\epsilon^{(n)} - \epsilon^{(n-1)}| < tol$
    Implicitly, $n = n + 1$
end while
Output: $\epsilon^{(n)}$

The combination of Equations (15)–(**??**)nd Eqn. (16), along with `PGREEDY` and degree tempering, results in the `GMVR` algorithm as presented in Alg. (5).

While not treated here, it is noted that Ref. [1] utilizes `GMVP` with a parameter dimension of 4.

In the following section we apply both `GMVP` and `GMVR` to the modeling of noiseless (up to roundoff error) data: the QNM frequencies of Kerr BHs, and the inner-products of the spherical and spheroidal harmonics. In each case, the underlying 1D parameter in each case will be the dimensionless BH spin, j_f.

Algorithm 5 GMVR, a degree tempered stepwise algorithm for multivariate rational modeling of scalar data.

Input: $\{x, f, \text{max\_degree} = 6, tol\}$
Define, $\boldsymbol{\lambda}_{bulk}$, the bulk symbol space using the n-fold cartesian inner-product of the power set of each basis symbol. This is the combined bulk for numerator and denominator symbols.
Define $\mathcal{A}_{\texttt{GMVR}}$ according to Alg. (4).
Given *max_order*, define, D, a list of allowed polynomial degrees (e.g. $\{0, 1, 2, 3, 4, 5, 6\}$)
for d **in** D **do**
    Define $\boldsymbol{\lambda}^{(d)}_{bulk}$ as all symbols from $\boldsymbol{\lambda}_{bulk}$ with degree less than or equal to current degree: $\boldsymbol{\lambda}^{(d)}_{bulk}$
    Using $\boldsymbol{\lambda}^{(d)}_{bulk}$, apply Alg. (1), PGREEDY, with $\mathcal{A}_{\texttt{GMVP}}$ to get symbol subset, $\boldsymbol{\lambda}^{(d)}_{opt}$ and estimator val, $\epsilon^{(d)}_{opt}$
    if $|\boldsymbol{\lambda}^{(d)}_{opt} - \boldsymbol{\lambda}^{(d-1)}_{opt}| < tol$ **then**
        break
    end if
end for
Output: $\boldsymbol{\lambda}^{(d)}_{opt}$

III. RESULTS

We present the application of GMVP and GMVR to the respective modeling of QNM frequencies, and harmonic mixing coefficients. While each case is an instance of modeling on a 1D domain, we note that higher dimensional cases have been treated elsewhere [1].

A. Modeling QNM frequencies using GMVP

In seeking to apply GMVP to select QNM frequencies, we wish to impose a zero-damping constraint, namely that some frequencies are real as $j_f \to 1$. We also wish the impose a domain transformation, $\kappa(j_f)$, such that $0 \leq \kappa \leq 1$ and the individual QNM frequencies are morphologically simplified.

For the domain transformation, inspection of QNM frequencies with $\ell \leq 5$ suggest that

$$\kappa(j_f) = \left(\ln(2 - j_f)/\ln(3)\right)^{1/(2-\ell+|m|)} \tag{17}$$

appropriately linearizes the sharp behavior of each frequency near $j_f = 1$.

For the zero-damping constraint, when considering a QNM frequency $\tilde{\omega}_{\ell mn}$, zero-damping at $j_f = 1$ implies that $\tilde{\omega}_{\ell mn}(\kappa \approx 0) - m/2 \propto \kappa$, where $m/2$ is the well known limiting value for each QNM frequencies real part as $j_f \to 1$. This implies that

$$\tilde{\omega}_{\ell mn} = m/2 + \kappa \sum_{j=1}^{J} c_j \kappa^k \,. \tag{18}$$

In the case of the non-zero damped QNMs, (e.g. $(\ell, m) = (3, 2)$), a more general polynomial form may be adopted, namely,

$$\tilde{\omega}_{\ell mn} = \sum_{j=0}^{J} c_j \kappa^k \,. \tag{19}$$

The polynomial content of Eqn. (18) and Eqn. (19) is determined by GMVP. Equations (20)–(28) display the resulting polynomial models. Although each model's fractional error is within 2%, each is error is dominated by well known nonlinear oscillations which are considered to be outside of the experimental accuracy of current GW efforts.

Fig. 1 displays select training points, as well as model fits for $\tilde{\omega}_{lmn}$'s real and imaginary parts. For the right and left panels, simple polynomial behavior of each curve is a result of the displayed linear domain in $\kappa(j_f)$. In the left panel, we have scaled $1/\tau_{\ell mn}$ by factors for $m/(n + 1/2)$ to place the QNMs with $n = 0$ and $n = 1$ at approximately the same scale.

$$\tilde{\Omega}_{220}(\kappa) = 1.0 + \kappa(1.5578e^{2.9031i} + 1.9510e^{5.9210i}\kappa + 2.0997e^{2.7606i}\kappa^2 + 1.4109e^{5.9143i}\kappa^3 + 0.4106e^{2.7952i}\kappa^4) \tag{20}$$

$$\tilde{\Omega}_{221}(\kappa) = 1.0 + \kappa(1.8709e^{2.5112i} + 2.7192e^{5.4250i}\kappa + 3.0565e^{2.2857i}\kappa^2 + 2.0531e^{5.4862i}\kappa^3 + 0.5955e^{2.4225i}\kappa^4) \tag{21}$$

$$\tilde{\Omega}_{330}(\kappa) = 1.5 + \kappa(2.0957e^{2.9650i} + 2.4696e^{5.9967i}\kappa + 2.6655e^{2.8176i}\kappa^2 + 1.7584e^{5.9327i}\kappa^3 + 0.4991e^{2.7817i}\kappa^4) \tag{22}$$

$$\tilde{\Omega}_{331}(\kappa) = 1.5 + \kappa(2.3391e^{2.6497i} + 3.1399e^{5.5525i}\kappa + 3.5916e^{2.3472i}\kappa^2 + 2.4490e^{5.4435i}\kappa^3 + 0.7004e^{2.2830i}\kappa^4) \tag{23}$$

$$\tilde{\Omega}_{440}(\kappa) = 2.0 + \kappa(2.6589e^{3.0028i} + 2.9783e^{6.0510i}\kappa + 3.2184e^{2.8775i}\kappa^2 + 2.1276e^{5.9897i}\kappa^3 + 0.6034e^{2.8300i}\kappa^4) \tag{24}$$

$$\tilde{\Omega}_{430}(\kappa) = 1.5 + \kappa(0.2050e^{0.5953i} + 3.1033e^{3.0162i}\kappa + 4.2361e^{6.0388i}\kappa^2 + 3.0289e^{2.8262i}\kappa^3 + 0.9084e^{5.9152i}\kappa^4) \tag{25}$$

$$\tilde{\Omega}_{550}(\kappa) = 2.5 + \kappa(3.2405e^{3.0279i} + 3.4906e^{6.0888i}\kappa + 3.7470e^{2.9212i}\kappa^2 + 2.4725e^{6.0365i}\kappa^3 + 0.6994e^{2.8766i}\kappa^4) \tag{26}$$

$$\tilde{\Omega}_{320}(\kappa) = 1.0225e^{0.0049i} + 0.2473e^{0.6653i}\kappa + 1.7047e^{3.1383i}\kappa^2 + 0.9460e^{0.1632i}\kappa^3 + 1.5319e^{5.7036i}\kappa^4 + 2.2805e^{2.6852i}\kappa^5 + 0.9215e^{5.8417i}\kappa^6 \tag{27}$$

$$\tilde{\Omega}_{210}(\kappa) = 0.5891e^{0.0435i} + 0.1890e^{2.2899i}\kappa + 1.1501e^{5.8101i}\kappa^2 + 6.0459e^{2.7420i}\kappa^3 + 11.1263e^{5.8441i}\kappa^4 + 9.3471e^{2.6694i}\kappa^5 + 3.0384e^{5.7915i}\kappa^6 \tag{28}$$

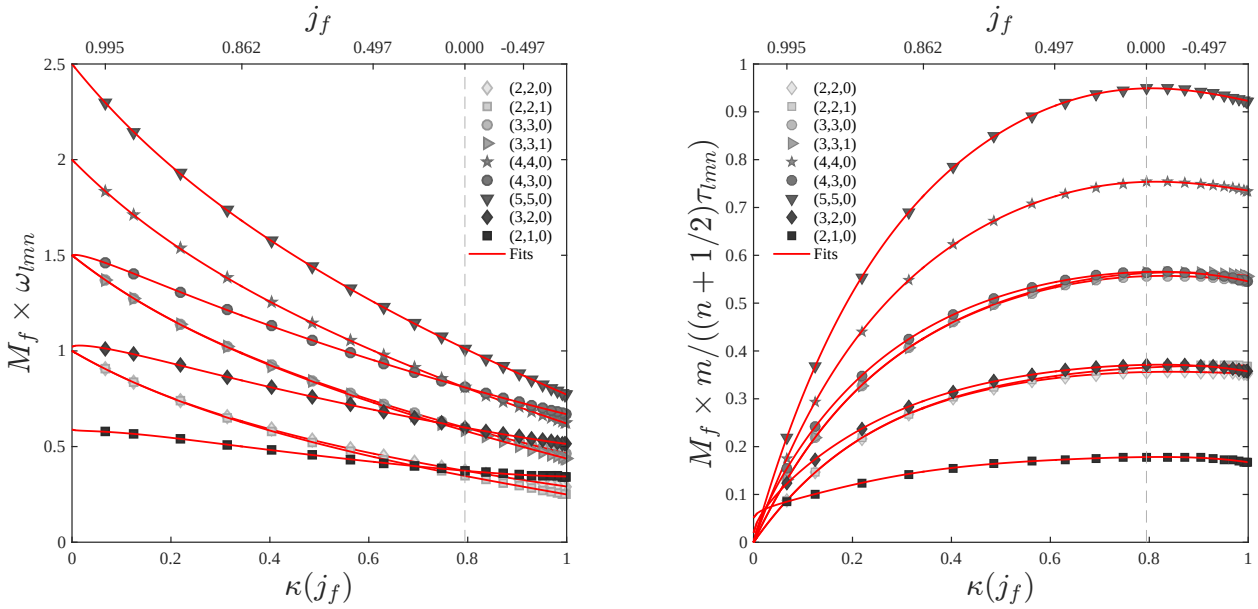

FIG. 1. Fits of dimensionless QNM central frequencies (solid lines) along with select numerical values (grey markers) computed using Leaver's method [2]. Before the application of $\kappa(\jmath)$, points are spaced between -0.995 and 0.995 according to 0.995 times the sin of a fiducial angle which is uniformly spaced between $-\pi/2$ and $\pi/2$. Values of $\jmath$ are shown in the upper axis for κ at $l = m$. The grey dashed line marks the value of κ where $\jmath = 0$. Fits of dimensionless QNM decay rates (solid lines) along with select numerical values (grey markers) computed using Leaver's method [2].

B. Modeling spherical-spheroidal inner-products using `GMVR`

$$\sigma_{22220} = 0.99733\, e^{6.2813i} + 0.0075336\, \frac{14.592\, e^{5.0601i}\,\kappa + (28.761\, e^{1.629i})\,\kappa^2 + (14.511\, e^{4.6362i})\,\kappa^3 + (1.9624\, e^{3.0113i})}{1 + 0.88674\, e^{3.0787i}\,\kappa + (1.002\, e^{0.13211i})\,\kappa^2 + (0.082148\, e^{5.6369i})\,\kappa^3} \tag{29}$$

$$\sigma_{21210} = 0.99716\, e^{6.2815i} + 0.0063542\, \frac{1.4345\times10^5\, e^{4.5061i}\,\kappa + (3.5469\times10^5\, e^{1.7327i})\,\kappa^2 + (2.4038\times10^5\, e^{5.1629i})\,\kappa^3 + (6026.9\, e^{1.8881i})}{1 + 73780\, e^{4.5545i}\,\kappa + (97494\, e^{1.398i})\,\kappa^2 + (34815\, e^{4.5623i})\,\kappa^3} \tag{30}$$

$$\sigma_{22221} = 0.99683\, e^{6.2782i} + 0.020758\, \frac{15.077\, e^{4.8323i}\,\kappa + (31.139\, e^{1.585i})\,\kappa^2 + (15.449\, e^{4.6727i})\,\kappa^3 + (0.71897\, e^{2.8084i})}{1 + 0.80592\, e^{3.3995i}\,\kappa + (0.69502\, e^{0.54275i})\,\kappa^2 + (0.35613\, e^{5.9545i})\,\kappa^3} \tag{31}$$

$$\sigma_{32320} = 0.99009\, e^{6.2804i} + 0.02369\, \frac{71893\, e^{1.2395i}\,\kappa + (1.7055\times10^5\, e^{5.0371i})\,\kappa^2 + (1.2947\times10^5\, e^{2.359i})\,\kappa^3 + (1935.5\, e^{4.668i})}{1 + 38206\, e^{1.2254i}\,\kappa + (35811\, e^{3.9618i})\,\kappa^2 + (8378.3\, e^{0.11726i})\,\kappa^3} \tag{32}$$

$$\sigma_{33331} = 0.99478\, e^{6.2688i} + 0.040478\, \frac{4.4113\, e^{1.2501i}\,\kappa + (11.588\, e^{0.27959i})\,\kappa^2 + (17.322\, e^{3.7904i})\,\kappa^3 + (0.67724\, e^{2.5797i})}{1 + 3.8782\, e^{2.2864i}\,\kappa + (3.4913\, e^{5.6655i})\,\kappa^2 + (1.0368\, e^{2.9082i})\,\kappa^3} \tag{33}$$

$$\sigma_{32221} = 0.02203\, e^{0.16452i} + 0.073233\, \frac{24.932\, e^{1.0181i}\,\kappa + (30.197\, e^{4.4047i})\,\kappa^2 + (11.274\, e^{2.981i})\,\kappa^3 + (2.4374\, e^{6.1959i})}{1 + 11.397\, e^{3.9953i}\,\kappa + (10.915\, e^{5.8025i})\,\kappa^2 + (7.2196\, e^{1.8176i})\,\kappa^3} \tag{34}$$

$$\sigma_{33330} = 0.99569\, e^{6.2785i} + 0.014546\, \frac{7.2112\, e^{0.62811i}\,\kappa + (6.5381\, e^{4.6216i})\,\kappa^2 + (4.451\, e^{2.9228i})\,\kappa^3 + (1.7113\, e^{2.9527i})}{1 + 1.4974\, e^{1.6687i}\,\kappa + (1.5288\, e^{5.3885i})\,\kappa^2 + (0.52114\, e^{2.5471i})\,\kappa^3} \tag{35}$$

$$\sigma_{32220} = 0.020598\, e^{0.04743i} + 0.06919\, \frac{2.7657\, e^{2.133i}\,\kappa + (3.9562\, e^{4.653i})\,\kappa^2 + (2.3364\, e^{2.6444i})\,\kappa^3 + (2.399\, e^{6.2767i})}{1 + 1.0595\, e^{4.7865i}\,\kappa + (0.91308\, e^{2.887i})\,\kappa^2 + (0.69468\, e^{0.1912i})\,\kappa^3} \tag{36}$$

$$\sigma_{43330} = 0.028112\, e^{0.048488i} + 0.086383\, \frac{12.087\, e^{0.47221i}\,\kappa + (30.626\, e^{3.3281i})\,\kappa^2 + (16.328\, e^{6.1785i})\,\kappa^3 + (2.3603\, e^{6.2662i})}{1 + 4.9638\, e^{3.5931i}\,\kappa + (6.2552\, e^{6.2001i})\,\kappa^2 + (1.4538\, e^{2.5539i})\,\kappa^3} \tag{37}$$

$$\sigma_{43430} = 0.98735\, e^{6.2795i} + 0.033028\, \frac{7.0084\times10^5\, e^{1.1067i}\,\kappa + (1.843\times10^6\, e^{4.8808i})\,\kappa^2 + (1.4367\times10^6\, e^{2.1412i})\,\kappa^3 + (13844\, e^{4.5601i})}{1 + 3.5667\times10^5\, e^{1.0149i}\,\kappa + (3.274\times10^5\, e^{3.7746i})\,\kappa^2 + (88621\, e^{0.10095i})\,\kappa^3} \tag{38}$$

$$\sigma_{44440} = 0.99478\, e^{6.2776i} + 0.024791\, \frac{6.5172\, e^{0.79835i}\,\kappa + (7.7748\, e^{4.2485i})\,\kappa^2 + (1.1577\, e^{1.5905i})\,\kappa^3 + (1.2434\, e^{2.9616i})}{1 + 0.44548\, e^{1.2496i}\,\kappa + (0.59437\, e^{5.6732i})\,\kappa^2 + (0.24743\, e^{2.8292i})\,\kappa^3} \tag{39}$$

$$\sigma_{55550} = 0.99434\, e^{6.2773i} + 0.03126\, \frac{6.5508\, e^{0.93398i}\,\kappa + (8.0558\, e^{4.2881i})\,\kappa^2 + (0.92971\, e^{1.0436i})\,\kappa^3 + (1.0904\, e^{2.9712i})}{1 + 0.23128\, e^{1.7666i}\,\kappa + (0.54958\, e^{5.9178i})\,\kappa^2 + (0.213\, e^{3.0092i})\,\kappa^3} \tag{40}$$

IV. DISCUSSION

[1] L. T. London, "Modeling ringdown II: non-precessing binary black holes," 2018.

[2] E. Leaver, "An Analytic representation for the quasi normal modes of Kerr black holes," *Proc.Roy.Soc.Lond.*, vol. A402, pp. 285–298, 1985.

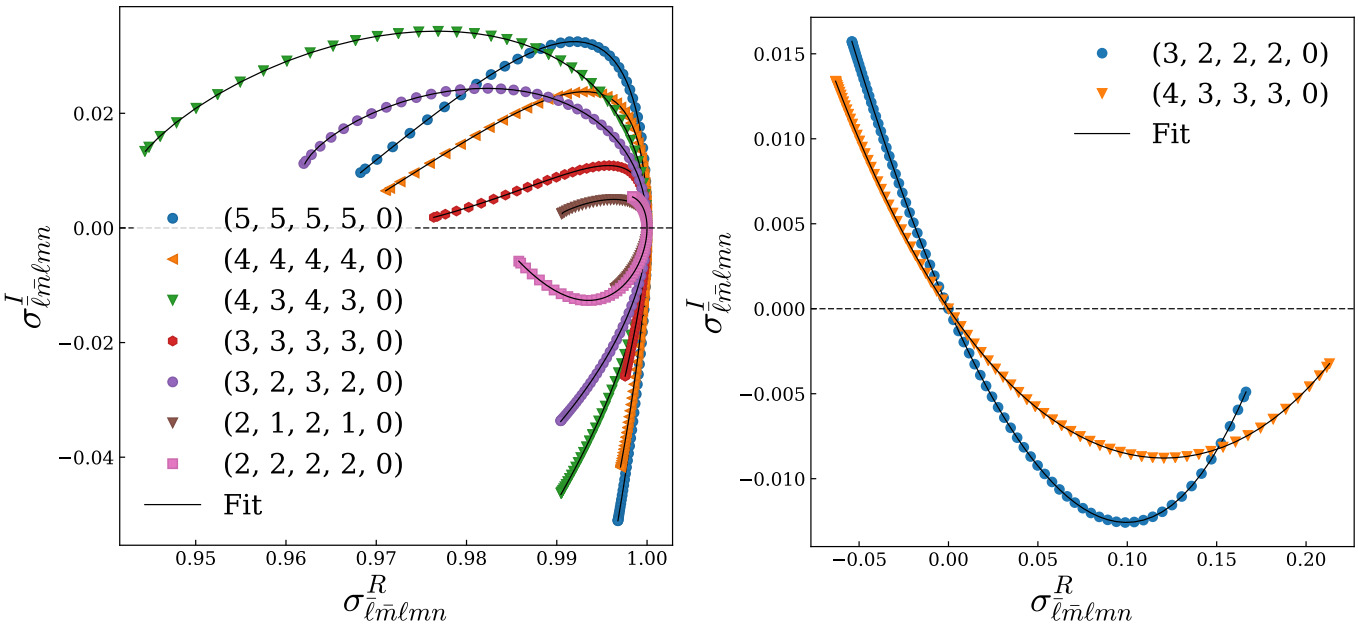

FIG. 2. Spherical-spheroidal harmonic mixing coefficients.